

Interp3R: Continuous-time 3D Geometry Estimation with Frames and Events

Shuang Guo^{1,2} , Filbert Febryanto^{1,2}, Lei Sun³ , and Guillermo Gallego^{1,2,4} 

¹ TU Berlin, Berlin, Germany

² Robotics Institute Germany, Berlin, Germany

³ INSAIT, Sofia University “St. Kliment Ohridski”, Sofia, Bulgaria

⁴ Einstein Center Digital Future and SCIOI Excellence Cluster, Berlin, Germany

Abstract. In recent years, 3D visual foundation models, pioneered by pointmap-based approaches such as DUSt3R, have attracted a lot of interest, achieving impressive accuracy and strong generalization across diverse scenes. However, these methods are inherently limited to recovering scene geometry only at the discrete time instants when images are captured, leaving the scene evolution during the blind time between consecutive frames largely unexplored. We introduce Interp3R, to the best of our knowledge, the first method that enhances pointmap-based models to estimate depth and camera poses at arbitrary time instants. Interp3R leverages asynchronous event data to interpolate pointmaps produced by frame-based models, enabling temporally continuous geometric representations. Depth and camera poses are then jointly recovered by aligning the interpolated pointmaps together with those predicted by the underlying frame-based models into a consistent spatial framework. We train Interp3R exclusively on a synthetic dataset, yet demonstrate strong generalization across a wide range of synthetic and real-world benchmarks. Extensive experiments show that Interp3R outperforms by a considerable margin state-of-the-art baselines that follow a two-stage pipeline of 2D video frame interpolation followed by 3D geometry estimation.

1 Introduction

Recent years have witnessed remarkable progress in 3D visual foundation models. Pointmap-based approaches such as DUSt3R [29] and its successors [18, 33] have demonstrated impressive performance in recovering scene geometry and camera poses from images, while exhibiting strong generalization across diverse environments. These models predict dense 3D pointmaps from input frames and enable various downstream tasks, including depth estimation and camera pose estimation. Despite their success, existing methods fundamentally operate on discrete-time image frames and can only recover scene geometry at the time instants when the frames are captured.

However, real-world scenes evolve continuously over time. The temporal gaps between consecutive frames inevitably introduce blind intervals during which the scene dynamics remain unobserved. This limitation becomes particularly severe

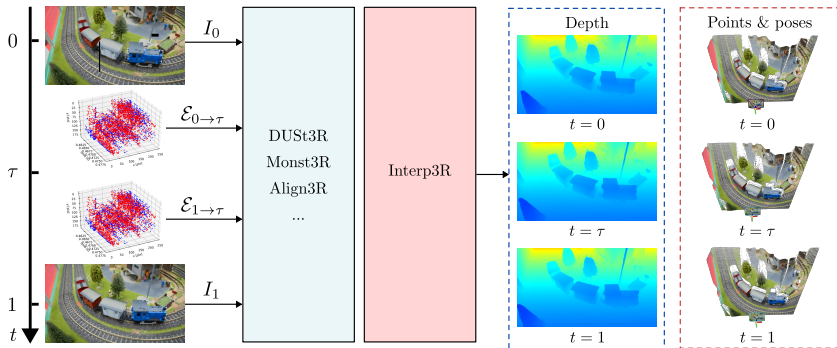


Fig. 1: The proposed method takes two images I_0, I_1 and the events between them \mathcal{E} as input (Left), and recovers the scene geometry (in the form of pointmaps) at an arbitrary time instant τ within the interval between the two images (Right). All available pointmaps can then be used to estimate depth maps and camera poses.

in scenarios with fast motion or large frame intervals, where significant geometric changes may occur between frames. As a result, current frame-based methods fail to provide temporally continuous representations of scene geometry.

Event cameras provide a promising solution to this problem. Unlike conventional cameras that capture images at fixed frame rates, event cameras asynchronously record per-pixel brightness changes with microsecond-level temporal resolution [1, 6]. This property allows them to capture fine-grained motion information between frames [10, 11], making them well suited for recovering scene evolution in continuous time [8, 9]. However, effectively integrating asynchronous event streams with modern pointmap-based models remains challenging. Events are sparse, noisy, and fundamentally different from frame-based representations, making it non-trivial to directly exploit them within existing 3D visual models.

In this paper, we propose Interp3R, a novel method that extends pointmap-based models to continuous-time 3D geometry estimation (Fig. 1). Given two frames processed by a frame-based model (e.g., DUST3R [29], MonST3R [33] or Align3R [18]), Interp3R leverages the co-captured event stream to interpolate pointmaps at arbitrary time instants between the frames. The interpolated pointmaps, together with those predicted from the input frames, are then aligned within a unified spatial framework in a novel coarse-to-fine manner in order to jointly recover depth and camera poses. This produces robust, progressively refined geometry estimation in continuous time across large temporal gaps.

We train Interp3R exclusively on synthetic data, yet the learned model generalizes well to a wide range of synthetic and real-world datasets. Extensive experiments demonstrate that Interp3R consistently outperforms baselines that follow a two-stage pipeline of 2D video frame interpolation followed by frame-based 3D geometry estimation. Our results show that incorporating event information enables accurate and temporally continuous reconstruction of scene geometry.

Our contributions can be summarized as follows:

Table 1: *Frame-based and Event-aided 3D Geometry / Video Depth Models.*

Method	Year	Type	Input	Video	Pose	Dynamic Scene	Continuous-time
VideoDepthAnything [4]	2025	FF	F	✓	✗	✓	✗
DepthAnything-v3 [17]	2025	FF	F	✓	✓	✓	✗
ChronoDepth [23]	2024	Diff	F	✓	✗	✓	✗
DepthCrafter [12]	2025	Diff	F	✓	✗	✓	✗
DUSt3R [29]	2024	PM	F	✓	✓	✗	✗
MonST3R [33]	2025	PM	F	✓	✓	✓	✗
Align3R [18]	2025	PM	F	✓	✓	✓	✗
EAG3R [30]	2025	PM	E+F	✓	✓	✓	✗
Interp3R (Ours)	2026	PM	E+F	✓	✓	✓	✓

¹ FF \equiv Feed-forward ViT; Diff \equiv Diffusion; PM \equiv Pointmap-based Model; F \equiv Frames; E \equiv Events.

1. We propose Interp3R, the *first method* that extends pointmap-based models to estimate scene geometry in continuous time, enabling the recovery of depth and camera poses at arbitrary time instants. It leverages asynchronous event data to interpolate pointmaps produced by frame-based models, and jointly recovers geometry by aligning the interpolated and frame-based pointmaps in a novel coarse-to-fine manner.
2. We show that Interp3R is compatible with different pointmap-based methods (e.g., MonST3R and Align3R), enhancing them to the continuous-time.
3. We train Interp3R exclusively on a synthetic dataset and demonstrate strong generalization across a variety of synthetic and real-world datasets. Extensive experiments show that our method outperforms baselines that follow a two-stage pipeline of 2D video frame interpolation followed by frame-based 3D geometry estimation.
4. We make the source code publicly available (upon acceptance).

2 Related Work

2.1 3D Geometry Estimation from Images and Videos

Recent years have witnessed significant progress in estimating scene geometry and camera motion from images. Early learning-based approaches mainly focused on predicting per-frame depth from monocular images [5, 15, 31, 32]. More recent works (Tab. 1) extend these models to videos in order to improve temporal consistency [4, 12, 23] and jointly recover camera motion [17].

Pointmap-based representations have emerged as a powerful paradigm for joint geometry and pose estimation. DUSt3R [29] introduces a pointmap representation that predicts aligned 3D point clouds from image pairs and implicitly recovers relative camera poses, demonstrating strong generalization across diverse scenes. Building on this idea, MonST3R [33] extends the framework to dynamic scenes by finetuning on dynamic datasets while introducing motion-aware global alignment. Align3R [18] further integrates monocular depth priors into the pointmap framework, combining feed-forward depth models and pointmap-based geometry estimation to improve temporal consistency.

Beyond per-frame geometry estimation, recent work has also explored modeling 3D motion between frames. DynaDUST3R [14] augments DUST3R with motion heads to predict 3D scene flow between two frames at an intermediate query time. Given two input images, the model predicts 3D displacement vectors that describe how points move in space, enabling the estimation of point trajectories across time. However, while DynaDUST3R can hallucinate sparse 3D motion between frames, it cannot recover camera poses or dense depth maps at intermediate timestamps

In summary, existing 3D geometry estimation approaches still operate at discrete frame timestamps and do not support continuous-time depth and pose estimation, leaving the blind time between frames unmodeled.

2.2 Event-based Video Frame Interpolation

Event-based video frame interpolation (EVFI) exploits the high temporal resolution of event cameras to synthesize intermediate frames between sparsely sampled images. TimeLens [28] and TimeLens++ [27] pioneer this direction by introducing a unified framework that estimates inter-frame motion from events and synthesizes intermediate frames accordingly. REFID [25] performs frame interpolation from blurry video inputs. CBMNet [16] improves motion estimation by jointly leveraging image and event modalities through cross-modal asymmetric bidirectional motion fields. TimeLens-XL [19] enables arbitrary-time frame interpolation by recursively decomposing large motions into smaller temporal steps. VDM-EVFI [3] explores a generative approach by adapting pretrained video diffusion models for event-based frame interpolation, benefiting from large-scale video priors.

In short, existing EVFI methods primarily focus on interpolation intermediate frames and remain limited to modeling 2D *appearance*. In contrast, our work directly interpolates 3D *geometry* in continuous time, recovering both scene structure and camera motion at arbitrary time instants.

2.3 Event-aided 3D Models

Beyond frame-based 3D geometry estimation, several recent works explore the fusion of event data to improve geometric estimation under fast motion or challenging imaging conditions. Thanks to their high temporal resolution and high dynamic range, event cameras provide complementary motion cues that can benefit 3D reconstruction.

For example, ADAE [21] integrates event streams into monocular depth models [31, 32] to improve robustness under extreme illumination and motion blur. It introduces event-guided spatial and temporal feature fusion modules that compensate for degraded frame information while preserving the strong generalization capabilities of pretrained depth foundation models. However, the method focuses on per-frame depth prediction and does not explicitly model temporal consistency. EAG3R [30] (penultimate row in Tab. 1) uses events to augment MonST3R for jointly estimating depth and camera poses in extreme-lighting

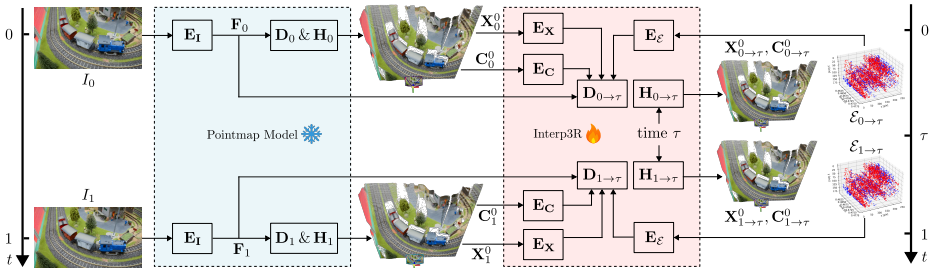


Fig. 2: Pipeline for pointmap prediction and interpolation. The pointmap model first takes as input two frames and outputs the source pointmaps. Interp3R then interpolates the pointmap at the arbitrary target time $\tau \in (0, 1)$ from two directions, with the first part ($0 \rightarrow \tau$, “forward”) and the second part ($1 \rightarrow \tau$, “backward”) event data.

scenes. By incorporating event-derived motion cues into pointmap alignment across frames, it improves robustness under extreme lighting conditions and fast motion. Nevertheless, the model still predicts geometry only at discrete frame timestamps and does not address geometry estimation between frames.

In summary, existing event-aided 3D models demonstrate that event cameras provide valuable complementary motion information for robust depth and pose estimation. However, these approaches remain restricted to discrete-time predictions tied to input frames, leaving the blind time between frames unexplored. In contrast, our work explicitly leverages event streams to interpolate geometric representations and recover depth and camera poses in continuous time, for the first time (last row of Tab. 1), to the best of our knowledge.

3 Method

3.1 Preliminaries

Our model achieves continuous-time estimation of depth and camera pose by interpolating the pointmaps produced by frame-based models like DUST3R. Here we begin with a brief review of DUST3R, as well as its follow-ups MonST3R and Align3R, which extends it from static to dynamic scenes.

Pointmap-based Geometry Estimation. Recent advances in pose-free 3D reconstruction adopt pointmap representations to directly regress dense geometry from image pairs. DUST3R predicts per-pixel 3D coordinates (pointmaps) for an image pair (I_0, I_1) using a transformer-based model:

$$(\mathbf{X}_0^0, \mathbf{X}_1^0) = \mathcal{F}_{\text{DUST3R}}(I_0, I_1), \quad (1)$$

where each pointmap assigns a 3D point to every pixel in the reference view. \mathbf{X}_0^0 and \mathbf{X}_1^0 indicate the pointmaps of I_0 and I_1 respectively, and both are expressed in the camera coordinates of I_0 . In general, \mathbf{X}_m^n indicates the pointmap of I_m expressed in the camera coordinates of I_n . These pairwise pointmaps encode relative geometry and can be aligned via a global optimization to recover consistent depth and camera poses across multiple views.

Extension to Dynamic Scenes. MonST3R extends DUST3R to dynamic videos by fine-tuning the pointmap prediction model on dynamic datasets. Specifically, MonST3R solves for a global state X_{global}^* by minimizing an objective composed of alignment, motion smoothness, and image-based flow constraints:

$$\mathcal{L}_{\text{MonST3R}}(X_{\text{global}}^*) = \mathcal{L}_{\text{align}} + w_{\text{smooth}}\mathcal{L}_{\text{smooth}} + w_{\text{flow}}\mathcal{L}_{\text{flow}}. \quad (2)$$

This formulation enables joint estimation of video depth and camera motion in the presence of scene dynamics.

Incorporating Monocular Depth Priors. Instead of relying solely on RGB images, Align3R injects per-frame monocular depth estimates to guide pointmap regression, providing stronger geometric initialization and improving depth accuracy and stability, especially for dynamic scenes.

3.2 Pairwise Pointmap Interpolation

As depicted in Fig. 2, a pointmap model (we use the latest model, Align3R, as the main model in this work) takes as input an image pair (I_0, I_1) and outputs the pairwise pointmaps $(\mathbf{X}_0^0, \mathbf{X}_1^0)$ as well as the corresponding confidence $(\mathbf{C}_0^0, \mathbf{C}_1^0)$ (i.e., a confidence value per 3D point).

Then, Interp3R takes as input these pointmap predictions, the RGB features $(\mathbf{F}_0, \mathbf{F}_1)$ of the two input frames (I_0, I_1) and the bidirectional event data $(\mathcal{E}_{0 \rightarrow \tau}, \mathcal{E}_{1 \rightarrow \tau})$, to interpolate the pointmaps $(\mathbf{X}_{0 \rightarrow \tau}^0, \mathbf{X}_{1 \rightarrow \tau}^0)$ at the target time $\tau \in (0, 1)$ from both directions $0 \rightarrow \tau$ and $1 \rightarrow \tau$. Note that both interpolated pointmaps are expressed in the camera coordinate of I_0 .

Incorporating Event Data and Pointmaps. The co-captured events between the two frames are divided into a forward set, $\mathcal{E}_{0 \rightarrow \tau}$, and a backward set, $\mathcal{E}_{\tau \rightarrow 1}$. The backward set $\mathcal{E}_{\tau \rightarrow 1}$ is formed by reversing the timestamps and polarities of all events, resulting in $\mathcal{E}_{1 \rightarrow \tau}$. After voxelization into spatiotemporal grids, denoted as $\mathcal{V}_{0 \rightarrow \tau}$ and $\mathcal{V}_{1 \rightarrow \tau}$, they are processed by the same event encoder $\mathbf{E}_{\mathcal{E}}$, as both of them describe motion from the source frame to the target interpolation time. Similarly, the predicted pointmaps $(\mathbf{X}_0^0, \mathbf{X}_1^0)$ and the corresponding confidence $(\mathbf{C}_0^0, \mathbf{C}_1^0)$ are also encoded by the same type of small vision transformer (ViT) encoders $(\mathbf{E}_{\mathbf{X}}$ and $\mathbf{E}_{\mathbf{C}}$) respectively. The extracted features from the pointmap predictions as well as the event voxels are then fused in the Interp3R decoders $(\mathbf{D}_{0 \rightarrow \tau}, \mathbf{D}_{1 \rightarrow \tau})$ using zero convolution [34].

The decoders and heads of Interp3R have the same structure as those of Align3R (but other choices are possible, as we show compatibility with MonST3R in Sec. 4.5), and are initialized by the weights of those of Align3R. Before being trained, Interp3R exactly outputs $(\mathbf{X}_0^0, \mathbf{X}_1^0)$, i.e., the pointmaps of the two input frames. As training iterates, the information about the source pointmaps and about the motion from the source to the target time τ are gradually injected to the Interp3R decoder. In this way, we do not abruptly change Align3R decoders and heads, instead, the predicted pointmaps are progressively transported from the source to the target time, which guarantees the stability of training.

Explicit Time Encoding. In many EVFI methods [19, 27, 28], forward and backward events are simply voxelized into spatiotemporal volumes with identical

channel dimensions and directly fed into the network for motion prediction. Under this formulation, the interpolation time τ is only implicitly encoded through temporal truncation of events, without being explicitly modeled.

However, such an implicit representation severely limits the model’s ability to reason about the target time. As a result, the interpolation quality becomes highly sensitive to the interpolation time, especially in the presence of non-uniform motion or complex scene dynamics. Inspired by [14], we explicitly incorporate a time encoding into the prediction heads, conditioning the model on the target interpolation time $\tau \in (0, 1)$. In this way, our method achieves more constant performance across different target times, as tested in Sec. 4.

Training Objective. As shown in Fig. 2, we only train the Interp3R component (i.e., the Align3R component is frozen), and use the confidence-aware scale-invariant 3D regression loss of DUST3R. We normalize the interpolated \mathbf{X}_τ and groundtruth pointmaps $\bar{\mathbf{X}}_\tau$ at $t = \tau$ using the scale factors calculated from the Align3R-predicted and groundtruth pointmaps at $t = 0$ and 1: $z = \text{norm}(\mathbf{X}_0, \mathbf{X}_1)$ and $\bar{z} = \text{norm}(\bar{\mathbf{X}}_0, \bar{\mathbf{X}}_1)$ ⁵, respectively. The final loss function for an image pair (I_0, I_1) is given by:

$$\mathcal{L}_{\text{interp}} = \sum_{v \in \{0, 1\}} \mathbf{C}_{v \rightarrow \tau} \left\| \frac{1}{z} \mathbf{X}_{v \rightarrow \tau} - \frac{1}{\bar{z}} \bar{\mathbf{X}}_{v \rightarrow \tau} \right\| - \alpha \log \mathbf{C}_{v \rightarrow \tau} \quad (3)$$

where $\mathbf{C}_{v \rightarrow \tau}$ is the pixel-wise confidence of $\mathbf{X}_{v \rightarrow \tau}$, and α is a hyper-parameter that controls the regularization term [29]. This loss function is the sum of interpolation errors (3D weighted Euclidean distance) from both temporal directions.

3.3 Coarse-to-Fine Global Alignment

After obtaining the pointmaps for all the frame and interpolation timestamps, we perform a coarse-to-fine global alignment to solve for the expected camera intrinsics, poses and depth at all those timestamps. We illustrate the proposed coarse-to-fine alignment in the case of one image pair in Fig. 3, where Θ_0 , Θ_τ and Θ_1 are the desired variables. In the coarse alignment, we align the source pointmaps produced by Align3R (in blue boxes) to calculate Θ_0 and Θ_1 , which is the same as the global alignment in Align3R. Note that dynamic scenes can be handled due to the capability of Align3R.

In the fine stage, we further align the interpolated pointmaps produced by Interp3R (in red boxes) with the source pointmaps to solve for the variables at the target time, Θ_τ , where Θ_0 and Θ_1 are initialized with the results of the coarse alignment and are still finetuned in the optimization. In practice, the target time τ can be set to any value between 0 and 1, and an arbitrary number of interpolated pointmaps can be fine-aligned. In this way, the continuous-time estimation of depth and pose is achieved.

Following DUST3R, we symmetrize every consecutive image pair (I_0, I_1) and event sets $(\mathcal{E}_{0 \rightarrow \tau}, \mathcal{E}_{1 \rightarrow \tau})$ to obtain a new pair (I_1, I_0) with $(\mathcal{E}_{1 \rightarrow \tau}, \mathcal{E}_{0 \rightarrow \tau})$. We also

⁵ where the variable with a bar denotes groundtruth and the norm operator computes the average distance between a set of points and the world origin

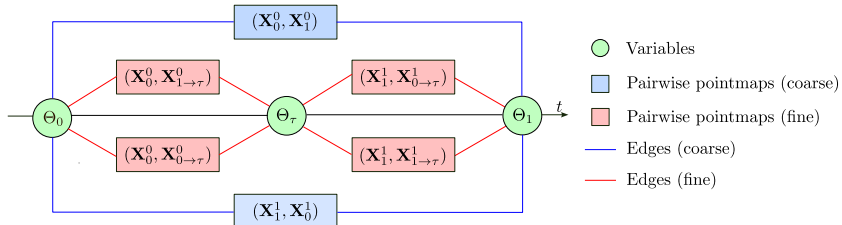


Fig. 3: Illustration of the coarse-to-fine global alignment. The components of the coarse alignment are plotted in blue, and those of the fine alignment are in red.

use this new pair to interpolate the pointmaps $(\mathbf{X}_{1 \rightarrow \tau}^1, \mathbf{X}_{0 \rightarrow \tau}^1)$, where the target time is $1 - \tau$ and the output pointmaps are expressed in the camera coordinate of I_1 . In this way, we obtain four pointmaps with confidence at the expected target position, which are inferred from two directions while expressed in two different coordinate systems. All these four measurements are then naturally fused according to pixel-wise confidence to obtain the estimation of depth and pose at $t = \tau$ in the fine-alignment stage.

4 Experiments

4.1 Experimental Setup

Implementation details. We train our model on six NVIDIA RTX A6000 GPUs with a total batch size of 12 for 50 epochs. We use the AdamW optimizer with a learning rate of 0.0001. Training is performed solely on the PointOdyssey [35] dataset. Each training sample consists of three images corresponding to timestamps $t = 0$, $t = \tau$, and $t = 1$. The temporal span of each triplet ranges from 2 to 10 frames. We also symmetrize the triplets for training to encourage the consistency of the trained model, as [29] does. Before training, we precompute all valid triplets and construct a uniformly distributed sampling pool by balancing both the left-right temporal spans and the relative position of the middle frame. This ensures that the model observes interpolation cases with different spans and relative positions evenly during training. During training, each epoch randomly samples 20,000 triplets from this pool to train the model.

Baselines. Similar to the evaluation of EVFI [28], we skip $k = \{1, 3, 7, 15\}$ frames, feed the remained frames as well as the event data in between to Interp3R to solve for depth and camera poses. Since our method is the first to address the target continuous-time depth and pose estimation tasks with events and frames, we create baselines based on concatenating state-of-the-art individual-task methods: we first leverage VFI methods (frame-based RIFE [13], and event-based Timelens [28] and VDM-EVFI [3]) to interpolate skipped frames, and then input all frames to Align3R to solve for depth and poses.

Table 2: Depth estimation results. **Best** and second best results are highlighted.

Dataset	Method	skip = 1		skip = 3		skip = 7		skip = 15	
		Abs Rel↓	$\delta < 1.25 \uparrow$						
PointOdyssey	RIFE	0.097	<u>0.925</u>	0.106	0.911	0.146	<u>0.891</u>	0.196	<u>0.846</u>
	TimeLens	<u>0.087</u>	<u>0.925</u>	<u>0.099</u>	<u>0.912</u>	0.142	0.858	0.215	0.777
	VDM-EVFI	0.108	0.889	0.113	0.875	<u>0.118</u>	0.861	<u>0.137</u>	0.839
	Interp3R (Ours)	0.069	0.948	0.067	0.952	0.074	0.948	0.099	0.896
Sintel	RIFE	0.381	0.538	0.478	0.532	0.515	0.522	0.580	0.507
	TimeLens	0.377	<u>0.548</u>	0.441	0.545	0.530	0.496	0.595	0.453
	VDM-EVFI	<u>0.366</u>	0.542	<u>0.390</u>	<u>0.553</u>	<u>0.397</u>	0.559	<u>0.424</u>	<u>0.543</u>
	Interp3R (Ours)	0.338	0.591	0.335	0.575	0.370	<u>0.534</u>	0.420	0.556
Bonn	RIFE	0.075	<u>0.956</u>	0.079	<u>0.952</u>	0.098	0.932	0.157	0.886
	TimeLens	0.077	<u>0.956</u>	0.082	0.949	0.104	0.922	0.226	0.758
	VDM-EVFI	<u>0.074</u>	0.959	<u>0.076</u>	0.955	0.076	0.956	0.076	0.956
	Interp3R (Ours)	0.069	0.954	0.070	0.946	0.067	<u>0.955</u>	<u>0.078</u>	<u>0.939</u>
TUM	RIFE	<u>0.110</u>	<u>0.876</u>	<u>0.114</u>	0.874	<u>0.130</u>	<u>0.856</u>	0.169	0.807
	TimeLens	0.112	0.872	0.116	0.868	0.133	0.827	0.189	0.730
	VDM-EVFI	0.133	0.824	0.128	0.828	<u>0.130</u>	0.834	<u>0.134</u>	<u>0.828</u>
	Interp3R (Ours)	0.103	0.879	0.101	0.880	0.101	0.880	0.101	0.881

4.2 Continuous-time Depth Estimation

Evaluation datasets. We evaluate our approach on both real-world and synthetic benchmarks. The real-world datasets include Bonn [20] and TUM dynamics [24], while the synthetic datasets include Sintel [2] and the validation split of PointOdyssey [35]. Since these datasets do not contain event data, we generate events for them using vid2e [7].

The Bonn dataset is a real-world RGB-D SLAM benchmark consisting of 24 dynamic sequences involving human activities such as moving boxes or interacting with balloons. Following the evaluation protocol of previous works [18, 33], we test our model on five sequences with an average length of 110 frames. The TUM dynamics dataset contains 8 dynamic scenes, from which 50 frames are selected per scene for evaluation. Sintel is a synthetic dynamic dataset composed of 23 sequences with roughly 50 frames each. The PointOdyssey validation set contains 15 dynamic scenes with multiple moving foreground objects, and the first 110 frames of each sequence are evaluated.

Evaluation metrics. Following prior works [18, 33], we first align the predicted depth maps to the groundtruth depth using a single scale and shift before computing the evaluation metrics. To make the comparison of temporal consistency fair across different methods, the scale and shift are estimated once for the entire image sequence rather than independently for each frame. We report two standard metrics: the absolute relative error (Abs Rel ↓) and the percentage of inlier pixels with $\delta < 1.25$ (↑). To highlight the performance on the interpolated frames, the metrics are calculated on the skipped frames.

Comparison with baseline methods. Table 2 reports the quantitative depth evaluation results under different frame gaps (skips). Our method consistently achieves the best performance on PointOdyssey, Sintel, and TUM across all settings. In particular, on PointOdyssey our approach improves the Abs Rel error over the best baseline by approximately 20%–37% depending on the skip value, while also achieving the highest $\delta < 1.25$ percentage. On Sintel and TUM, our method similarly yields the lowest Abs Rel and the highest inlier ratio across

all skip values with the only exception of skip = 7 on Sintel, demonstrating clear advantages over the baselines that sequentially perform 2D VFI and 3D geometry estimation. On the Bonn dataset, our method achieves the best performance on half of the evaluated metrics, and for the remaining metrics the gap to the best method is very small ($< 3\%$), indicating competitive performance.

We also observe that the performance of RIFE and TimeLens degrades significantly as the frame gap increases. This behavior is expected since RIFE only predicts the exact middle frame ($\tau = 0.5$), and larger skips require recursively interpolating additional frames, leading to noticeable error accumulation. TimeLens explicitly relies on linear optical flow for frame synthesis, and as the skip increases, the motion between frames becomes more complex and non-linear, which makes accurate interpolation more difficult. Among the baselines, VDM-EVFI is the most robust to increasing skip values and generally achieves the strongest performance. However, it relies on a large video diffusion model with strong priors, containing more than 3B parameters.

In contrast, our method demonstrates strong robustness across different frame gaps and interpolation positions. The performance remains nearly constant across skip values on the Bonn and TUM datasets. A noticeable increase in error only occurs on PointOdyssey and Sintel when the skip increases from 7 to 15, which is likely due to the significantly faster camera and object motion in these datasets.

4.3 Continuous-time Pose Estimation

Evaluation datasets. For camera pose evaluation, we largely follow the protocol used in Align3R and its preceding works. The evaluation is conducted on two real-world datasets, Bonn and TUM dynamics, and one synthetic dataset, Sintel. For the Bonn dataset, following prior works, we evaluate on five sequences and select 30 frames from each sequence for pose estimation. For the Sintel dataset, we adopt the same filtering strategy as previous methods and exclude sequences that are static or only exhibit simple linear motion, resulting in 14 test sequences. Our evaluation on the TUM dynamics dataset differs slightly from previous protocols. Instead of downsampling 30 frames from 90-frame sequences, as done in earlier works [18, 33], we directly use the same 50 frames selected for depth evaluation. This is because our method naturally operates on temporally sparse frames due to frame skipping during inference.

Evaluation metrics. Following prior studies [18, 33], we report three commonly used metrics: ATE \downarrow (Absolute Trajectory Error), RTE \downarrow (Relative Translation Error), and RRE \downarrow (Relative Rotation Error). ATE measures the discrepancy between the estimated trajectory and the groundtruth trajectory after alignment. RTE and RRE quantify the average local translation and rotation errors, respectively, computed between consecutive poses.

Comparison with baseline methods. Table 3 reports the pose estimation results under different frame skips. Our method consistently achieves the best performance in terms of rotation accuracy across all datasets and skip settings. Specifically, Interp3R significantly outperforms all competing methods in terms of RRE, with relative improvements ranging from approximately 23% to

Table 3: Camera pose evaluation. **Best** and second best results are highlighted.

Dataset	Method	skip = 1			skip = 3			skip = 7			skip = 15		
		ATE _l	RTE _l	RRE _l	ATE _l	RTE _l	RRE _l	ATE _l	RTE _l	RRE _l	ATE _l	RTE _l	RRE _l
Sintel	RIFE	<u>0.301</u>	0.104	<u>1.259</u>	<u>0.292</u>	0.115	1.290	<u>0.328</u>	0.146	1.675	0.434	0.157	2.547
	TimeLens	0.321	0.114	1.265	0.385	0.174	1.412	0.566	0.175	2.410	0.599	<u>0.141</u>	3.719
	VDM-EVFI	0.319	0.127	1.314	0.339	<u>0.128</u>	<u>1.193</u>	0.405	<u>0.148</u>	<u>1.351</u>	<u>0.379</u>	0.118	<u>1.496</u>
	Interp3R (Ours)	0.224	<u>0.111</u>	0.907	0.263	0.150	0.916	0.284	0.179	0.921	0.302	0.202	1.079
Bonn	RIFE	<u>0.011</u>	<u>0.007</u>	<u>0.749</u>	<u>0.012</u>	0.007	<u>0.746</u>	<u>0.013</u>	0.007	0.827	<u>0.015</u>	<u>0.008</u>	<u>0.782</u>
	TimeLens	<u>0.011</u>	0.008	0.762	<u>0.012</u>	<u>0.008</u>	0.765	0.015	<u>0.009</u>	<u>0.769</u>	0.017	0.010	1.482
	VDM-EVFI	0.016	0.011	0.816	0.017	0.011	0.792	0.016	0.010	0.772	0.019	0.010	0.835
	Interp3R (Ours)	0.007	0.006	0.424	0.008	0.007	0.428	0.009	0.007	0.449	0.009	0.006	0.494
TUM	RIFE	0.006	0.002	<u>0.438</u>	0.006	0.002	0.491	0.006	0.002	0.659	<u>0.007</u>	0.003	0.930
	TimeLens	0.006	<u>0.003</u>	0.475	0.006	0.002	<u>0.466</u>	<u>0.007</u>	<u>0.003</u>	0.478	0.011	<u>0.004</u>	1.561
	VDM-EVFI	<u>0.007</u>	<u>0.003</u>	0.495	0.006	<u>0.003</u>	0.468	<u>0.007</u>	<u>0.003</u>	<u>0.451</u>	0.006	0.003	<u>0.450</u>
	Interp3R (Ours)	0.009	0.004	0.226	<u>0.012</u>	0.006	0.234	0.012	0.006	0.259	0.010	0.005	0.325

50% compared to the best competing baseline. On Bonn, our method achieves the best results in terms of all metrics across every skip setting, demonstrating consistently superior performance. On Sintel, our approach also obtains the lowest ATE across all skip settings, outperforming the second-best method by approximately 10%–26%. This indicates that our method maintains accurate trajectory estimation even under large frame skips. For TUM, the translation errors of all methods are extremely small and nearly indistinguishable (ATE \approx 0.006–0.012 and RTE \approx 0.002–0.006 across all settings), suggesting that camera translation is very limited in this dataset. Instead, rotational motion dominates the camera movement. In this case, our method consistently achieves the lowest RRE, demonstrating its superior capability in estimating camera orientation.

4.4 Qualitative Results

A qualitative comparison of the estimated depth maps on the Bonn dataset are presented in Fig. 4. For all baseline methods, there are obvious artifacts at the edges of the moving man (marked in red boxes). This implies that the inaccuracy of the 2D VFI results is significantly amplified in the 3D geometry estimation, which leads to unreasonable and temporally inconsistent depth values. Although the percentage of such pixels is not very big, it could severely affect downstream tasks (e.g., robotic navigation and scene reconstruction). In contrast, our method produces spatially smooth and temporally consistent depth estimation. Note that our method does not interpolate frames; we present the skipped RGB frames for $t = \tau$ and use them to better visualize the points in Figs. 4 to 6.

We also present qualitative results on the DAVIS [22] dataset. Similarly, we generate synthetic events for the DAVIS dataset with vid2e. As shown in Fig. 5, we input the images at $t = 0$ and $t = 1$ and the events in-between to our method, which estimates depth and camera poses for all five timestamps, where $t = \{0.25, 0.5, 0.75\}$ are the skipped frames. It turns out that our method outputs precise poses and temporally consistent depth maps, which leads to precise points.

Next, Fig. 6 presents qualitative results on the EDS [11] dataset, which are estimated from real images and events. The fine textures in the scene are recov-

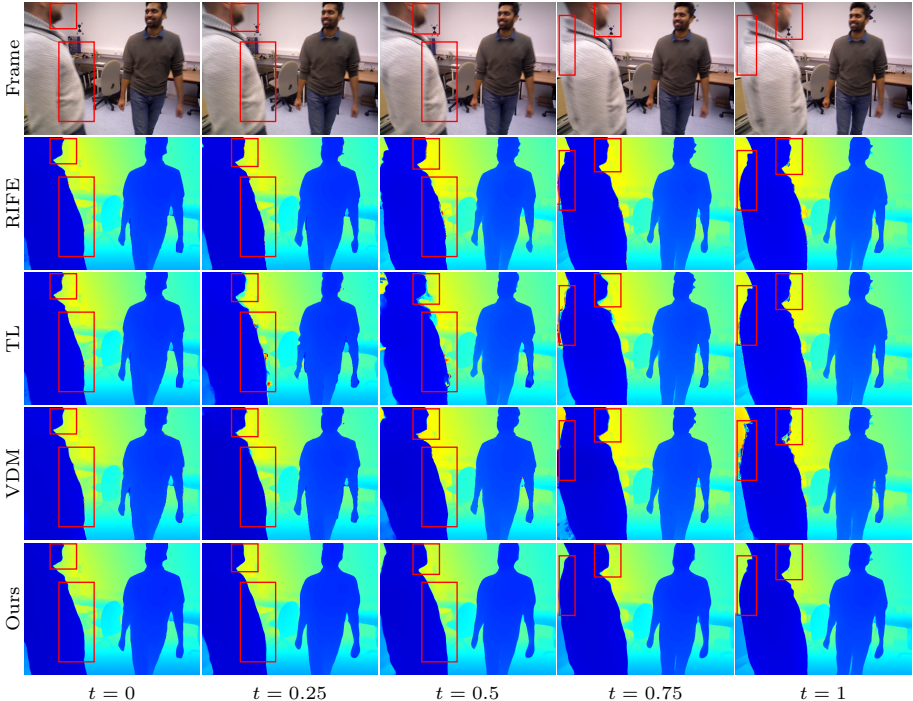


Fig. 4: Qualitative comparison of depth estimation on the Bonn dataset (skip = 3).

Table 4: Ablation studies. Results of depth evaluation on the PointOdyssey dataset.

Method	skip = 1		skip = 3		skip = 7		skip = 15	
	Abs Rel \downarrow	$\delta < 1.25 \uparrow$	Abs Rel \downarrow	$\delta < 1.25 \uparrow$	Abs Rel \downarrow	$\delta < 1.25 \uparrow$	Abs Rel \downarrow	$\delta < 1.25 \uparrow$
w/o events	0.073	0.945	0.078	0.942	0.100	0.926	0.153	0.855
w/o time encoding	0.107	0.901	0.104	0.909	0.106	0.913	0.117	0.898
MonST3R + Interp3R	0.090	0.915	0.090	0.910	0.097	0.883	0.108	0.876
Align3R + Interp3R	0.069	0.948	0.067	0.952	0.074	0.948	0.099	0.896

ered very well in the depth map at $t = 0.5$. It shows that our model generalizes well to real images and events, despite being trained only on synthetic data.

4.5 Ablation Studies

Finally, we conduct ablation studies to show the effects of event data, interpolation time encoding, and Interp3R’s compatibility with other frame-based pointmap models (e.g., MonST3R). Results of depth estimation on PointOdyssey and camera pose estimation on Sintel are presented in Tabs. 4 and 5, respectively.

Effects of Event Data. First, we train Interp3R without the input events and the event encoder $\mathbf{E}_{\mathcal{E}}$, with all other settings the same. As shown in Tab. 4, depth accuracy is still comparable when skip = 1 and skip = 3, but as the skip increases, the values degrade rapidly. It turns out that the motion cues conveyed by the event data are vital when the frame gap is large. The same conclusion

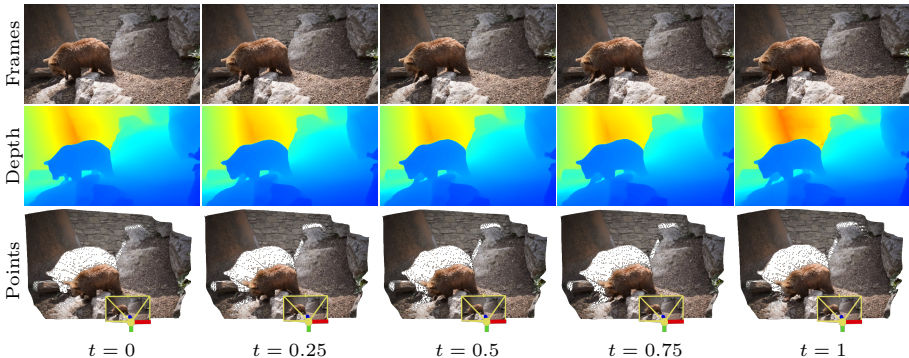


Fig. 5: Qualitative results on the DAVIS dataset (skip = 3).

Table 5: Ablation studies. Results of camera pose evaluation on the Sintel dataset.

Method	skip = 1			skip = 3			skip = 7			skip = 15		
	ATE↓	RTE↓	RRE↓									
w/o events	0.222	0.102	0.909	0.285	0.178	0.916	0.338	0.217	0.914	0.404	0.220	0.927
w/o time encoding	0.280	0.148	0.931	0.304	0.168	0.931	0.254	0.169	2.731	0.315	0.212	2.744
MonST3R + Interp3R	0.218	0.087	0.918	0.247	0.135	0.948	0.251	0.131	0.924	0.336	0.172	0.918
Align3R + Interp3R	0.224	0.111	0.907	0.263	0.150	0.916	0.284	0.179	0.921	0.302	0.202	1.079

can be drawn from Tab. 5, where pose accuracy errors grow significantly as the skip value increases.

Effects of Time Encoding. Second, we train Interp3R without the encoding of interpolation time, with all other settings the same. In this case, the estimated depth and poses are not as sensitive to the skip value as the “no-event” model, but they are less accurate than the full model.

Compatibility with MonST3R. Third, we replace Align3R, with which Interp3R is trained, by its concurrent work MonST3R, to provide source pointmap predictions, yielding a variant: MonST3R + Interp3R. In this test, Interp3R directly takes as input MonST3R predictions, and solves for the depth and camera poses, without finetuning. According to Tabs. 4 and 5, this variant shows comparable depth accuracy (Align3R has higher depth accuracy than MonST3R [18]) as the original model, while in many cases outperforming it in terms of ATE and RTE. This shows that Interp3R is compatible with other pointmap models besides Align3R. In other words, it can be used in a plug-n-play manner, enhancing the capability of pointmap models to continuous time.

4.6 Limitations

Despite its effectiveness, our approach has limitations. First, Interp3R performs pointmap interpolation directly on the outputs produced by the underlying frame-based model. When the source pointmaps are unreliable, e.g., due to motion blur or challenging illumination conditions in the input frames, the interpolation quality may also degrade. This issue could be mitigated by leveraging event data to enhance the input images before geometry estimation, e.g., through

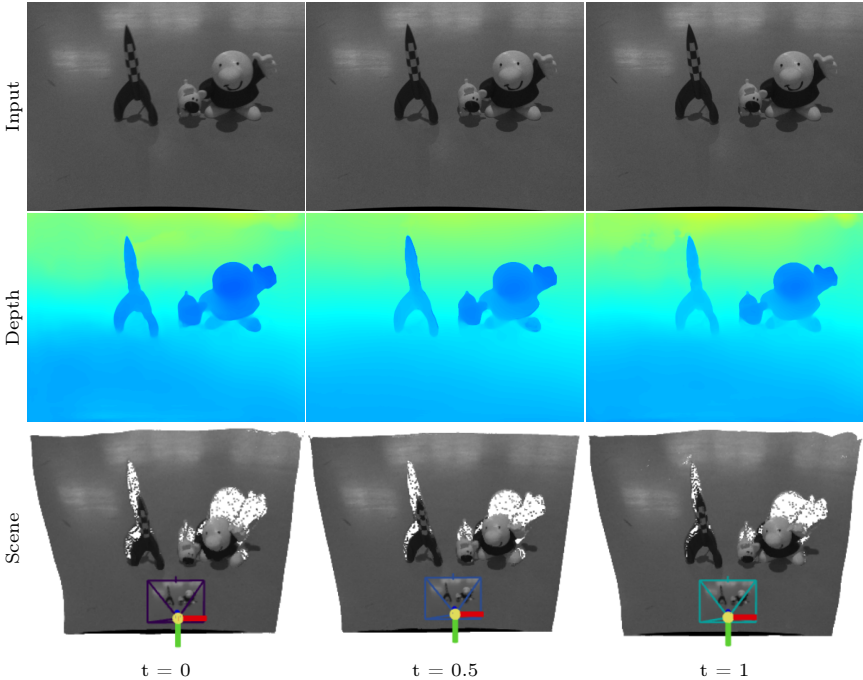


Fig. 6: Qualitative results on the EDS dataset (skip=1).

event-guided deblurring or image enhancement, which could improve the quality of the predicted pointmaps and consequently benefit the interpolation process.

Second, the proposed method relies on event streams to capture motion cues between frames. However, when the scene contains flickering or rapidly changing light sources, the resulting events may not correspond to true scene motion. In such cases, the event signals can introduce artifacts and affect the interpolation results. This limitation could be addressed by detecting and removing such non-motion events, or by injecting additional knowledge.

5 Conclusion

In this paper, we introduced Interp3R, a novel framework that extends pointmap-based models to continuous-time 3D geometry estimation. By leveraging asynchronous event data, our method interpolates intermediate pointmaps between input frames, enabling the recovery of depth and camera poses at arbitrary time instants. The interpolated pointmaps are jointly aligned with those predicted by frame-based models within a unified spatial framework, allowing temporally continuous reconstruction of scene geometry. Extensive experiments show that our approach consistently outperforms state-of-the-art baselines that rely on a two-stage pipeline of video frame interpolation followed by frame-based geometry estimation. We hope our work highlights the potential of combining event-based

sensing with modern 3D visual foundation models, and opens new directions for temporally continuous 3D perception in dynamic environments.

A Supplementary Material

A.1 Additional Implementation Details

ViT encoders for pointmaps, confidence and events. For each input modality, including the pointmap \mathbf{X} , confidence \mathbf{C} , and event voxel representation \mathcal{V} , we first apply a standard patch embedding operation to partition the input into a sequence of patches:

$$\mathbf{W}' = \text{PatchEmbed}(\mathbf{W}), \quad (4)$$

where $\mathbf{W}' \in \mathbb{R}^{H' \times W' \times C}$ denotes the patch-embedded representation of the input modality \mathbf{W} . The resulting patch tokens are then processed by a Vision Transformer encoder to extract hierarchical feature representations $\hat{F}^{(1)}, \hat{F}^{(2)}, \dots, \hat{F}^{(s)}$. These multi-scale features are subsequently injected into the Interp3R decoder to facilitate feature aggregation and refinement.

Feature fusion using zero convolution. To preserve the prediction capability of the original pointmap model, we adopt zero convolution layers [34] to fuse the extracted features within the Interp3R decoder:

$$\hat{E}^{(l)} = \text{ZeroConv}(\hat{F}^{(l)}) + E^{(l)}, \quad l = 1, 2, \dots, s, \quad (5)$$

where $E^{(l)}$ denotes the feature map produced by the Align3R decoder at the l -th layer, while $\hat{E}^{(l)}$ represents the fused feature map after incorporating the features derived from the input modalities (pointmaps, confidence maps, and events).

Coarse-to-fine global alignment. In both coarse and fine stages of the proposed global alignment, we optimize the parameters for 300 iterations using the Adam optimizer. The learning rate is initialized at 0.01 and follows a linear decay schedule throughout the optimization process. The flow loss in (2) is only used in the coarse alignment, where the optical flow is provided by a pretrained RAFT model [26].

References

1. Brandli, C., Berner, R., Yang, M., Liu, S.C., Delbruck, T.: A 240x180 130dB 3 μ s latency global shutter spatiotemporal vision sensor. *IEEE J. Solid-State Circuits* **49**(10), 2333–2341 (2014). <https://doi.org/10.1109/JSSC.2014.2342715>
2. Butler, D.J., Wulff, J., Stanley, G.B., Black, M.J.: A naturalistic open source movie for optical flow evaluation. In: *Eur. Conf. Comput. Vis. (ECCV)*. pp. 611–625 (2012). https://doi.org/10.1007/978-3-642-33783-3_44
3. Chen, J., Feng, B.Y., Cai, H., Wang, T., Burner, L., Yuan, D., Fermuller, C., Metzler, C.A., Aloimonos, Y.: Repurposing pre-trained video diffusion models for event-based video interpolation. In: *IEEE Conf. Comput. Vis. Pattern Recog. (CVPR)*. pp. 12456–12466 (Jun 2025). <https://doi.org/10.1109/cvpr52734.2025.01162>

4. Chen, S., Guo, H., Zhu, S., Zhang, F., Huang, Z., Feng, J., Kang, B.: Video Depth Anything: Consistent depth estimation for super-long videos. In: IEEE Conf. Comput. Vis. Pattern Recog. (CVPR). pp. 22831–22840 (2025). <https://doi.org/10.1109/CVPR52734.2025.02126>
5. Fu, X., Yin, W., Hu, M., Wang, K., Ma, Y., Tan, P., Shen, S., Lin, D., Long, X.: GeoWizard: Unleashing the diffusion priors for 3D geometry estimation from a single image. In: Eur. Conf. Comput. Vis. (ECCV). pp. 241—258 (Sep 2024). https://doi.org/10.1007/978-3-031-72670-5_14
6. Gallego, G., Delbruck, T., Orchard, G., Bartolozzi, C., Tabata, B., Censi, A., Leutenegger, S., Davison, A., Conradt, J., Daniilidis, K., Scaramuzza, D.: Event-based vision: A survey. IEEE Trans. Pattern Anal. Mach. Intell. **44**(1), 154–180 (2022). <https://doi.org/10.1109/TPAMI.2020.3008413>
7. Gehrig, D., Gehrig, M., Hidalgo-Carrió, J., Scaramuzza, D.: Video to Events: Recycling video datasets for event cameras. In: IEEE Conf. Comput. Vis. Pattern Recog. (CVPR). pp. 3583–3592 (2020). <https://doi.org/10.1109/CVPR42600.2020.00364>
8. Guo, S., Gallego, G.: CMax-SLAM: Event-based rotational-motion bundle adjustment and SLAM system using contrast maximization. IEEE Trans. Robot. **40**, 2442–2461 (2024). <https://doi.org/10.1109/TRO.2024.3378443>
9. Guo, S., Gallego, G.: Event-based photometric bundle adjustment. IEEE Trans. Pattern Anal. Mach. Intell. **47**(10), 9280–9297 (2025). <https://doi.org/10.1109/TPAMI.2025.3586497>
10. Guo, S., Hamann, F., Gallego, G.: Unsupervised joint learning of optical flow and intensity with event cameras. In: Int. Conf. Comput. Vis. (ICCV). pp. 7980–7989 (2025). <https://doi.org/10.48550/arXiv.2503.17262>
11. Hidalgo-Carrió, J., Gallego, G., Scaramuzza, D.: Event-aided direct sparse odometry. In: IEEE Conf. Comput. Vis. Pattern Recog. (CVPR). pp. 5781–5790 (Jun 2022). <https://doi.org/10.1109/CVPR52688.2022.00569>
12. Hu, W., Gao, X., Li, X., Zhao, S., Cun, X., Zhang, Y., Quan, L., Shan, Y.: DepthCrafter: Generating consistent long depth sequences for open-world videos. In: CVPR. pp. 2005–2015 (2025). <https://doi.org/10.1109/CVPR52734.2025.00193>
13. Huang, Z., Zhang, T., Heng, W., Shi, B., Zhou, S.: Real-time intermediate flow estimation for video frame interpolation. In: Eur. Conf. Comput. Vis. (ECCV). pp. 624—642 (2022). https://doi.org/10.1007/978-3-031-19781-9_36
14. Jin, L., Tucker, R., Li, Z., Fouhey, D., Snavely, N., Holynski, A.: Stereo4D: Learning how things move in 3D from internet stereo videos. In: IEEE Conf. Comput. Vis. Pattern Recog. (CVPR). pp. 10497–10509 (2025). <https://doi.org/10.1109/CVPR52734.2025.00982>
15. Ke, B., Obukhov, A., Huang, S., Metzger, N., Dautt, R.C., Schindler, K.: Repurposing diffusion-based image generators for monocular depth estimation. In: IEEE Conf. Comput. Vis. Pattern Recog. (CVPR). pp. 9492–9502 (2024). <https://doi.org/10.1109/CVPR52733.2024.00907>
16. Kim, T., Chae, Y., Jang, H.K., Yoon, K.J.: Event-based video frame interpolation with cross-modal asymmetric bidirectional motion fields. In: IEEE Conf. Comput. Vis. Pattern Recog. (CVPR). pp. 18032–18042 (Jun 2023). <https://doi.org/10.1109/CVPR52729.2023.01729>
17. Lin, H., Chen, S., Liew, J.H., Chen, D.Y., Li, Z., Shi, G., Feng, J., Kang, B.: Depth Anything 3: Recovering the visual space from any views. arXiv preprint arXiv:2511.10647 (2025)
18. Lu, J., Huang, T., Li, P., Dou, Z., Lin, C., Cui, Z., Dong, Z., Yeung, S.K., Wang, W., Liu, Y.: Align3R: Aligned monocular depth estimation for dynamic videos.

- In: IEEE Conf. Comput. Vis. Pattern Recog. (CVPR). pp. 22820–22830 (2025). <https://doi.org/10.1109/CVPR52734.2025.02125>
19. Ma, Y., Guo, S., Chen, Y., Xue, T., Gu, J.: TimeLens-XL: Real-time event-based video frame interpolation with large motion. In: Eur. Conf. Comput. Vis. (ECCV). pp. 178—194 (Oct 2024). https://doi.org/10.1007/978-3-031-72907-2_11
 20. Palazzolo, E., Behley, J., Lottes, P., Giguère, P., Stachniss, C.: ReFusion: 3D reconstruction in dynamic environments for RGB-D cameras exploiting residuals. In: IEEE/RSJ Int. Conf. Intell. Robot. Syst. (IROS). pp. 7855–7862 (2019). <https://doi.org/10.1109/IROS40897.2019.8967590>
 21. Peng, S., Xiong, Y., Zhou, H., Shi, Z., Liu, H., Chen, G., Yan, L., Chang, Y.: Adapting depth anything to adverse imaging conditions with events. arXiv e-prints (2026)
 22. Perazzi, F., Pont-Tuset, J., McWilliams, B., Van Gool, L., Gross, M., Sorkine-Hornung, A.: A benchmark dataset and evaluation methodology for video object segmentation. In: IEEE Conf. Comput. Vis. Pattern Recog. (CVPR). pp. 724–732 (2016). <https://doi.org/10.1109/CVPR.2016.85>
 23. Shao, J., Yang, Y., Zhou, H., Zhang, Y., Shen, Y., Guizilini, V., Wang, Y., Poggi, M., Liao, Y.: Learning temporally consistent video depth from video diffusion priors. In: IEEE Conf. Comput. Vis. Pattern Recog. (CVPR). pp. 22841–22852 (2025). <https://doi.org/10.1109/CVPR52734.2025.02127>
 24. Sturm, J., Engelhard, N., Endres, F., Burgard, W., Cremers, D.: A benchmark for the evaluation of RGB-D SLAM systems. In: IEEE/RSJ Int. Conf. Intell. Robot. Syst. (IROS). pp. 573–580 (Oct 2012). <https://doi.org/10.1109/IROS.2012.6385773>
 25. Sun, L., Sakaridis, C., Liang, J., Sun, P., Cao, J., Zhang, K., Jiang, Q., Wang, K., Van Gool, L.: Event-based frame interpolation with ad-hoc deblurring. In: IEEE Conf. Comput. Vis. Pattern Recog. (CVPR). pp. 18043–18052 (2023). <https://doi.org/10.1109/CVPR52729.2023.01730>
 26. Teed, Z., Deng, J.: RAFT: Recurrent all-pairs field transforms for optical flow. In: Eur. Conf. Comput. Vis. (ECCV). pp. 402–419 (2020). https://doi.org/10.1007/978-3-030-58536-5_24
 27. Tulyakov, S., Bochićchio, A., Gehrig, D., Georgoulis, S., Li, Y., Scaramuzza, D.: Time Lens++: Event-based frame interpolation with parametric non-linear flow and multi-scale fusion. In: IEEE Conf. Comput. Vis. Pattern Recog. (CVPR). pp. 17734–17743 (Jun 2022). <https://doi.org/10.1109/CVPR52688.2022.01723>
 28. Tulyakov, S., Gehrig, D., Georgoulis, S., Erbach, J., Gehrig, M., Li, Y., Scaramuzza, D.: Time lens: Event-based video frame interpolation. In: IEEE Conf. Comput. Vis. Pattern Recog. (CVPR). pp. 16150–16159 (Jun 2021). <https://doi.org/10.1109/CVPR46437.2021.01589>
 29. Wang, S., Leroy, V., Cabon, Y., Chidlovskii, B., Revaud, J.: DUST3R: Geometric 3D vision made easy. In: IEEE Conf. Comput. Vis. Pattern Recog. (CVPR). pp. 20697–20709 (2024). <https://doi.org/10.1109/CVPR52733.2024.01956>
 30. Wu, X., Yu, Y., Lyu, X., Huang, Y., Wang, B., Zhang, B., Wang, Z., Qi, X.: EAG3R: Event-augmented 3D geometry estimation for dynamic and extreme-lighting scenes. arXiv e-prints (2025)
 31. Yang, L., Kang, B., Huang, Z., Xu, X., Feng, J., Zhao, H.: Depth anything: Unleashing the power of large-scale unlabeled data. In: IEEE Conf. Comput. Vis. Pattern Recog. (CVPR). pp. 10371–10381 (2024). <https://doi.org/10.1109/CVPR52733.2024.00987>
 32. Yang, L., Kang, B., Huang, Z., Zhao, Z., Xu, X., Feng, J., Zhao, H.: Depth anything V2. In: Adv. Neural Inf. Process. Syst. (NeurIPS) (2024)

33. Zhang, J., Herrmann, C., Hur, J., Jampani, V., Darrell, T., Cole, F., Sun, D., Yang, M.H.: MonST3R: A simple approach for estimating geometry in the presence of motion. In: Int. Conf. Learn. Representations (ICLR) (2025)
34. Zhang, L., Rao, A., Agrawala, M.: Adding conditional control to text-to-image diffusion models. In: Int. Conf. Comput. Vis. (ICCV). pp. 3813–3824 (2023). <https://doi.org/10.1109/ICCV51070.2023.00355>
35. Zheng, Y., Harley, A.W., Shen, B., Wetzstein, G., Guibas, L.J.: PointOdyssey: A large-scale synthetic dataset for long-term point tracking. In: Int. Conf. Comput. Vis. (ICCV). pp. 19798–19808 (2023). <https://doi.org/10.1109/ICCV51070.2023.01818>